JOURNAL OF OPTOELECTRONICS AND ADVANCED MATERIALS Vol. 9, No. 8, August 2007, p. 2504 - 2508

Fractal and fracture mechanics analyses of fatigue fracture surfaces of metallic materials

T. SAKAI*
Department of Mechanical Engineering, Takamatsu National College of Technology, 355 Chokushi, Takamatsu, Kagawa 761-8058 Japan

In this study, fatigue crack propagation tests were performed to obtain fatigue fracture surfaces on compact tension type specimens of A5052 aluminum alloy and S25C carbon steel. The fatigue fracture surfaces were observed using a scanning laser microscope system. Based on the digital data thus obtained, an imaginary fracture surface was reconstructed in a three-dimensional (3D) space using a personal computer. Fractal analysis proposed by Mandelbrot was applied to such 3D surfaces and a hyperbola model was accepted to represent the Richardson effect. Because of the Richardson effect thus analyzed, fractal features were distinguished in the fracture surface irregularity. Results demonstrated that the geometrical irregularity of the surface was well evaluated by combining the fractal dimension and additional indices termed as "indices of fracture surface nature", and that the fractal dimension and the additional indices were associated with the stress intensity factor range of ΔK.

(Received June 6, 2007; accepted June 27, 2007)

Keywords: Fractal, Richardson effect, Self-similarity, Fatigue fracture surface, Surface irregularity, Fractography, Fracture mechanics, Scanning laser microscope observation

1. Introduction

To analyze the irregularity of shapes and time-dependent phenomena, many researchers have developed and used various methods such as Fourier analysis and some conventional procedures such as stochastic processes. The concept of fractals proposed by Mandelbrot [1] is useful to quantify the above irregularity; it has been applied to various fields in both science and technology [2–5].

On the other hand, several kinds of high-resolution microscopy have been used in recent years to observe the nature of the fracture surface in a three-dimensional (3D) space: scanning laser microscopy (SLM), scanning tunnel microscopy (STM) and atomic force microscopy (AFM). However, definite procedures to quantify the irregularity of the fracture surfaces have not been established yet.

As reported in earlier papers [68], we proposed a new analytical method to quantify surface irregularities through application of the fractal concept. In addition, the surface irregularities of the tensile fracture surfaces and the mechanically finished surfaces were evaluated using this method. In the present study, this method is modified and expanded to analyze the surface irregularity of the fatigue fracture surfaces. Moreover, particular attention is given here to investigating the relationship between surface irregularities and the fracture mechanics parameter of ΔK.

2. Specimen and fatigue crack propagation tests

2.1 Specimens and Fatigue Crack Propagation Behavior

Materials used in this study are A5052 aluminum alloy and S25C carbon steel in JIS material codes. Mechanical properties of these materials obtained by tensile tests are listed in Table 1. Fatigue crack propagation tests were performed using a hydraulic servo fatigue-testing machine to create fatigue fracture surfaces on a compact tension type specimen [9,10] standardized in ASTM. The frequency was fixed to 50 Hz; two different stress ratios of $R = 0.1$ and 0.5 were selected. Fatigue fracture surfaces were examined using an SLM system, as explained in precedent studies [11,12]. Fatigue crack propagation was examined using an optical microscope with 100× magnification.

Table 1. Mechanical properties of materials.

Material	Yield stress σ_y (MPa)	0.2% Proof stress $\sigma_{0.2}$ (MPa)	Tensile strength σ_B (MPa)	Elongation δ (%)	Reduction of area φ (%)
A5052	-	225	268	19.8	43.4
S25C	333	-	506	35.5	59.8

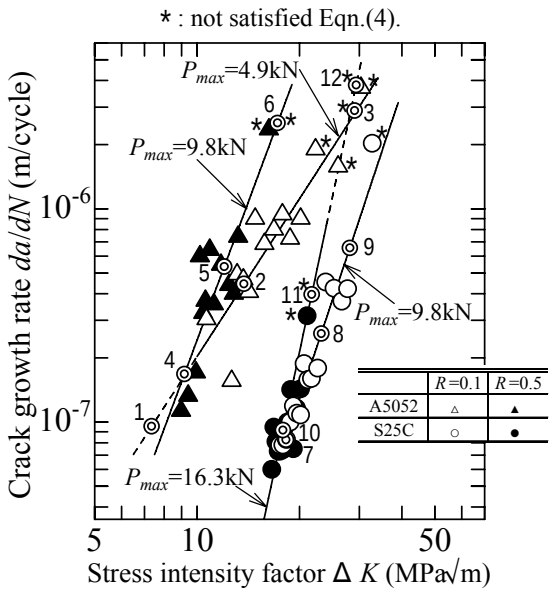

Fig. 1. Relationships between stress intensity factor range ΔK and crack growth rate da/dN.

Fig. 1 shows, based on the crack propagation behavior thus observed, relationships between the stress intensity factor range ΔK and the crack growth rate d*a*/d*N*. It is noteworthy that only one specimen was assigned to each series of the fatigue crack propagation test. In this figure, each solid line is determined to provide the least-squares for the respective data points. The fatigue crack propagation behavior is well represented by the following expression [13]:

$$\frac{da}{dN} = C(\Delta K)^m \tag{1}$$

where

$$\Delta K = \frac{\Delta P}{BW^{\frac{1}{2}}} \times f(\alpha) \tag{2}$$

$$f(\alpha) = \frac{(2+\alpha)(0.886+4.64\alpha-13.32\alpha^2+14.72\alpha^3-5.6\alpha^4)}{(1-\alpha)^{\frac{3}{2}}} \tag{3}$$

and $f(\alpha)$ is the modification coefficient depending on the specimen configuration of $\alpha = a / W$. Furthermore, ΔP and a respectively represent the load range and the crack length B and W are the specimen thickness and width; they are B = 16mm and W = 32mm for the present specimens.

When the linear fracture mechanics are applied to fatigue crack propagation behavior, the following conditions of small scale yielding [14] must always be satisfied.

$$W - a \geq \frac{4}{\pi}\left(\frac{K_{\max}}{\sigma_y}\right)^2 \tag{4}$$

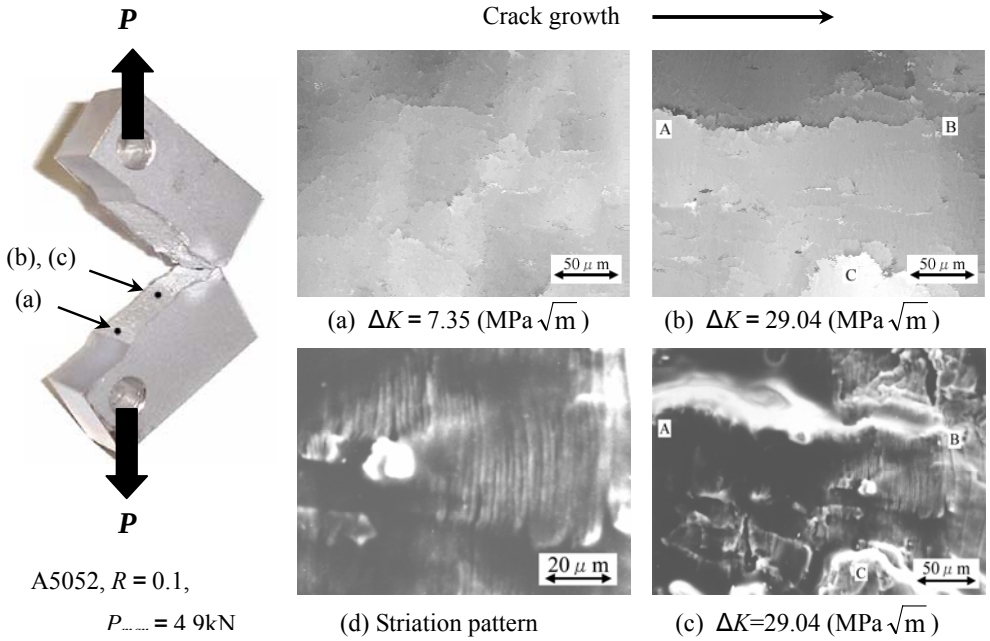

Fig. 2. (a), (b)SLM and (c), (d)SEM micrographs of fatigue fracture surface.

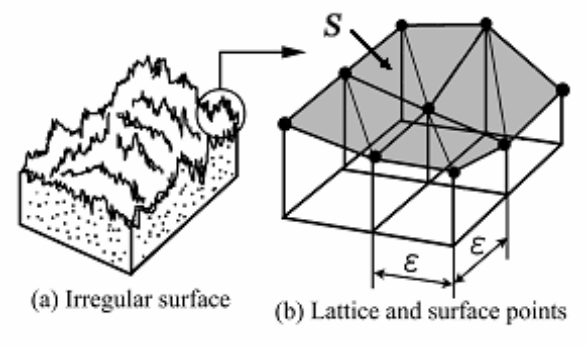

Fig. 3. Reconstruction of imaginary fracture surface by multifacet surface.

Therein, σ_y is the yield stress of the materials, and K_{max} is the maximum stress intensity factor calculated by substituting the maximum load P_{max} into ΔP in Eq. (2). In this study, we have $\sigma_{0.2} = 225$MPa for the A5052 specimen and $\sigma_y = 333$MPa for the S25C specimen, as shown in Table 1. Based on calculations at every stage of the crack propagation, almost all experimental points in Fig. 1 satisfy the above condition, except for a few points shown by "*", which appear in the crack high-growth rate region.

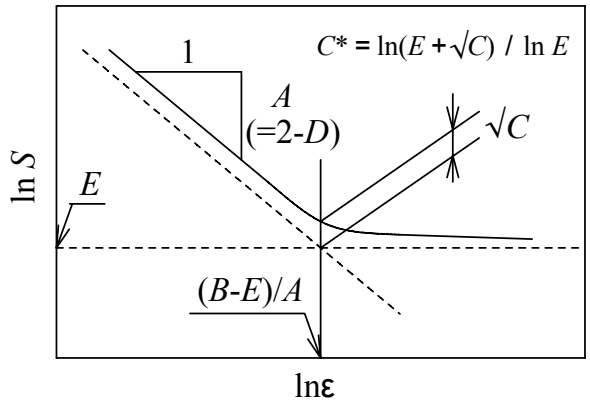

Fig. 4. Schematics of lnε - ln S relationship.

2.2 Observation of fatigue fracture surfaces

Fatigue fracture surfaces were observed using scanning laser microscopy (SLM). Comparison with scanning electronic microscopy (SEM) observations shows that the present SLM offers some advantages such that 3D numerical data are obtained directly in real time. These data are fundamentally convenient for fractal analyses performed in this study.

Table 2. Numerical list of analytical results (P_{max} = 4.9kN).

Material	ΔK	Mag.	Mark	D	$(B-E)/A$	C^*
A5052 (Fatigue) R=0.1	29.04 MPa$\sqrt{m}$	500	◎	2.42	51.5	1.13
		1250	▽	2.37	26.8	1.17
		2500	◇	2.16	7.4	1.04
S25C (Fatigue) R=0.1	26.33 MPa$\sqrt{m}$	500	○	2.34	42.5	1.12
		1250	△	2.38	19.1	1.14
		2500	□	2.34	11.1	1.19
S35C (Tension)	-	500	•	2.39	36.7	1.11
		1250	▲	2.65	27.1	1.34
		2500	■	2.78	20.7	1.36

As examples of SLM observations, micrographs of the fatigue fracture surface of A5052 aluminum alloy taken at ×1250 magnification are shown in Figs. 2 (a) and 2 (b). For comparison, SEM micrographs of the same area are also shown in Fig. 2 (c) and the striation pattern is again observed with still higher resolution, as shown in Fig. 2 (d). In these SLM micrographs, the bright part indicates a high position on the real surface, whereas a dark part indicates a low position. The actual height (total depth) in Fig. 2 (a) is 64μm and that in Fig. 2 (b) is 122 μ m, respectively. For SLM observation with magnification of ×1250, a square area of 161.5μm×161.5 μm is defined as a sample space to analyze the fracture surface irregularity. This area is replaced by a 200pixel× 200pixel square on the CRT screen. Based on the digital data thus obtained, the imaginary fracture surface was reconstructed in a 3D space, as illustrated in Fig. 3. Fractal analyses were performed on geometrical irregularities of such an imaginary fracture surface.

3. Analytical procedure

As reported in precedent studies [6, 7], geometrical irregularities of the tensile fracture surfaces and the mechanically finished surfaces were well evaluated using the "fractal" method. If a surface has a fractal nature, the following equation pertains between the total area of imaginary fracture surface S and the measuring unit length ε:

$$\ln S = \ln F + (2 - D)\ln\varepsilon \tag{5}$$

where D is the fractal dimension. This dimension is calculable from the slope of the regression line for the $\ln\varepsilon$ - $\ln S$ relationship, as shown in Fig. 4. The value of D is always in $D\gamma 2.0$ because the regression line must have a negative slope. Surface area S changes depending on the unit length of ε, and the effect of ε on the surface area S is the so-called "Richardson effect" [15].

Usually, the linear Richardson effect is confirmed within a limited range of ε, so that the effect is no longer represented by the linear expression in other areas of ε. The Richardson effect in the entire region of ε should be represented by a different type of expression. Accordingly, the following hyperbola-type expression [16] is proposed here:

$$(\ln S - E)(\ln S + A\ln\varepsilon - B) = C \tag{6}$$

Definitions of all parameters in this expression are indicated schematically in Fig. 4. Fractal dimension D is calculable from the slope of A as $D = 2 - A$. Other parameters such as B, C, and E are termed the "indices of fracture surface nature" in this paper because these parameters well reflect the fracture surface's geometrical characteristics.

4. Analytical results and discussion

4.1 Analytical results and self-similarity of the fatigue fracture surface

As examples of the Richardson effect, the fracture surface area S measured on A5052 alloy and S25C steel specimens is shown as functions of the unit length ε in Figs. 5 (a) and 5 (b). For comparison, the analytical results of the tensile fracture surface [6] are also shown using small solid symbols in Fig. 5 (b). The fractal dimension and each index of the fracture surface nature analyzed for the respective SLM micrographs are listed in Table 2. Fractal dimensions are calculated from the slope of each regression line for individual magnification. Each horizontal dashed line indicates the level of a perfect flat surface that has $D = 2.0$ for every magnification of the SLM observation. These figures show that $\ln\varepsilon - \ln S$ relationships for fatigue fracture surfaces of the objective materials are well represented by the expression in hyperbola type in Eq. (6).

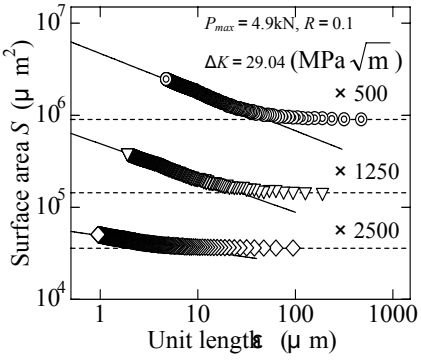

(a) A5052 aluminum alloy

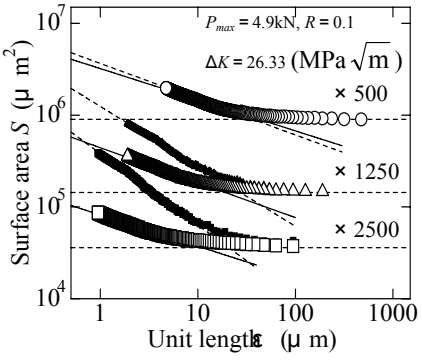

(b) S25C carbon steel

Fig. 5. $\ln\varepsilon - \ln S$ relationships for A5052 aluminum alloy and S25C carbon steel under $R = 0.1$.

If the analytical object has a fractal nature, then the irregularity is well evaluated by the fractal dimension and must have characteristics of self-similarity [1]. In Table 2, the values of D are shown to be almost constant for the fracture surfaces of S25C carbon steel in a wide resolution range. However, in the case of A5052 aluminum alloy, the fractal dimension tends to decrease at higher magnification of × 2500. Therefore, self-similarity cannot be confirmed in the entire resolution range, depending on the material. A similar trend was apparent for the fracture surfaces that failed under $R = 0.5$.

4.2 Connection between surface irregularity and fracture mechanics

Relationships between the stress intensity factor range ΔK and the fractal dimension D are plotted in Fig. 6. Each number attached to the bracket is a code number to be linked to the corresponding number in Fig. 1. Figure 6 (a) shows that the fractal dimension tends to increase with increased ΔK in the lower resolution, but the value remains constant at higher resolution. Consequently, the macroscopic irregularity on the fracture surface increases with increased ΔK, whereas the microscopic irregularity has no effect on ΔK. In contrast, in Fig. 6 (b), the fractal dimension tends to increase as ΔK is increased in the entire magnification range. Therefore, the macroscopic and the microscopic irregularities on the fracture surface of S25C increase with increased ΔK.

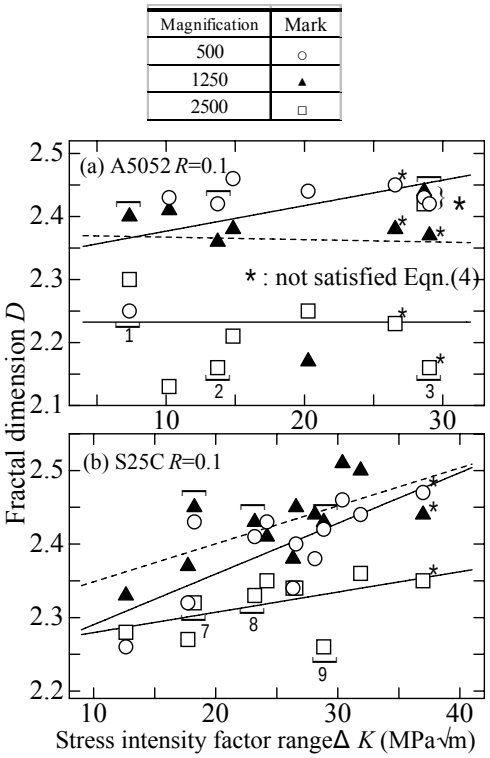

Fig. 6. Relationships between stress intensity factor range ΔK and fractal dimension D.

Furthermore, in the relationships between the ΔK and index of fracture surface nature $(B - E) / A$, the value of $(B - E) / A$ tends to increase irrespective of the magnification range as ΔK increases. Especially, this trend is distinct in the lower magnification range. The fractal dimension and each index of fracture surface nature were associated with the stress intensity factor range of ΔK.

5. Conclusions

An analytical procedure was developed to evaluate the surface irregularity of the fatigue fracture surfaces for A5052 aluminum alloy and S25C carbon steel by applying concepts of fractal and a curve fitting techniques.

(1) Fatigue fracture surfaces of the present metallic materials have a fractal nature. Especially, the fracture surfaces of S25C carbon steel under stress ratios of $R = 0.1$ and 0.5 have complete self-similarity over a wide range of resolutions.
(2) To evaluate the geometrical irregularity of the fracture surface, one should combine the fractal dimension and additional indices termed as "indices of fracture surface nature".
(3) The fractal dimension and each index of fracture surface nature are associated with the stress intensity factor range ΔK, yielding a key parameter in the fracture mechanics approach to assess crack propagation.

References

[1] B. B. Mandelbrot, The Fractal Geometry of Nature. W. H. Freeman and Company, (1983), p. 109.
[2] Z. P. Bazant, (1998). Structural Safety and Reliability **2**, 1255 (1998).
[3] T. Sakai, M. Fujikawa, Transaction of Japan Society of Mechanical Engineering. **A-64**, 2271 (1998).
[4] M. Tanaka, Journal of Materials Science Research International **47**, 169 (1998).
[5] M. Tsuda, et al., Journal of Materials Science Research International **40**, 1066 (1991).
[6] T. Sakai, et al., Transaction of Japan Society of Mechanical Engineering **A-66**, 741. (2000).
[7] T. Sakai, et al., Transaction of Japan Society of Mechanical Engineering **A-64,** 1104 (1998).
[8] T. Sakai, Optoel. Adv. Mat. – Rapid Comm. **1**(5), 235 (2007).
[9] J. E. Srawley, International Journal of Fracture **12**, 475 (1976).
[10] K. Murakami, et al., Stress Intensity Factor Handbook, Pergamon **1**, 18 (1987).
[11] T. Oide, Journal of Materials Science Research International **44**, 262 (1995).
[12] K. Masubuchi, Welding Journal **71**, 69 (1992).
[13] P. C. Paris, et al., Transaction of the ASME, Journal of Basic Engineering **85**, 528 (1963).
[14] ASTM E647-93, Standard Test Method for Measurement of Fatigue Crack Growth Rate, (1993).
[15] L. F. Richardson, General System Yearbook **6**, 139 (1961).
[16] S. Nishijima, Transaction of Japan Society of Mechanical Engineering **A-46**, 1303 (1990).

*Corresponding author: sakai@takamatsu-nct.ac.jp